

Soft Nanomembrane Sensors and Flexible Hybrid Bioelectronics for Wireless Quantification of Blepharospasm

Musa Mahmood, Shinjae Kwon , Gamze Kilic Berkmen, Yun-Soung Kim, Laura Scorr, H. A. Jinnah, and Woon-Hong Yeo, Senior Member, IEEE

Abstract—Blepharospasm (BL) is characterized by involuntary closures of the eyelids due to spasms of the orbicularis oculi muscle. The gold standard for clinical evaluation of BL involves visual inspection for manual rating scales. This approach is highly subjective and error prone. Unfortunately, there are currently no simple quantitative systems for accurate and objective diagnostics of BL. Here, we introduce a soft, flexible hybrid bioelectronic system that offers highly conformal, gentle lamination on the skin, while enabling wireless, quantitative detection of electrophysiological signals. Computational and experimental studies of soft materials and flexible mechanics provide a set of key fundamental design factors for a lowprofile bioelectronic system. The nanomembrane soft electrodes, mounted around the eyes, are capable of accurately measuring clinical symptoms, including the frequency of blinking, the duration of eye closures during spasms, as well as combinations of blinking and spasms. The use of a deep-learning, convolutional neural network, with the bioelectronics offers objective, real-time classification of

Manuscript received November 8, 2019; revised January 9, 2020; accepted January 22, 2020. Date of publication February 21, 2020; date of current version October 20, 2020. The work of W.-H. Yeo was supported in part by NSF (#1939094), NextFlex funded by the Department of Defense, in part by the Nano-Material Technology Development Program through the National Research Foundation of Korea funded by the Ministry of Science, ICT, in part by Future Planning under Grant 2016M3A7B4900044, and in part by the Georgia Research Alliance based in Atlanta, Georgia. The work of H. A. Jinnah was supported in part by the Dystonia Coalition, a consortium that was funded by NCATS and NINDS under Grant TR0001456 and in part by the Rare Diseases Clinical Research Network of the NIH. (M. Mahmood and S. Kwon contributed equally to this work.) (Corresponding author: Woon-Hong Yeo.)

Musa Mahmood, Shinjae Kwon, and Yun-Soung Kim are with the George W. Woodruff School of Mechanical Engineering, Institute for Electronics and Nanotechnology, Georgia Institute of Technology.

Gamze Kilic Berkmen, Laura Scorr, and H. A. Jinnah are with the Department of Neurology and Human Genetics, School of Medicine, Emory University.

Woon-Hong Yeo is with the George W. Woodruff School of Mechanical Engineering, Institute for Electronics and Nanotechnology, Georgia Institute of Technology, Atlanta, GA 30332 USA and also with the Wallace H. Coulter Department of Biomedical Engineering, Neural Engineering Center, Parker H. Petit Institute for Bioengineering and Biosciences, Center for Flexible and Wearable Electronics Advanced Research, Institute for Materials, Institute for Robotics and Intelligent Machines, Georgia Institute of Technology, Atlanta, GA 30332 USA (e-mail: whyeo@gatech.edu).

This article has supplementary downloadable material available at http://ieeexplore.ieee.org, provided by the authors.

Digital Object Identifier 10.1109/TBME.2020.2975773

key pathological features in BL. The wearable bioelectronics outperform the conventional manual clinical rating, as shown by a pilot study with 13 patients. *In vivo* demonstration of the bioelectronics with these patients indicates the device as an easy-to-use solution for objective quantification of BL.

Index Terms—Soft bioelectronics, stretchable electrodes, flexible hybrid electronics, blepharospasm, electrophysiology, quantitative diagnostics.

I. INTRODUCTION

LEPHAROSPASM (BL), a form of focal dystonia, is Characterized by involuntary activations and movements of periocular muscles [1]. The main problem is spasms of the orbicularis oculi muscle, but other muscle groups may also be involved [1], [2]. Such spasms manifest in a variety of ways that include excessive blinking, varying duration of eye closures, and eye closures that are partial or complete. Additional symptoms may involve apraxia of eyelid opening, and dystonia in other body parts, such as the lower face [1]. Often, subjects with BL are unable to control their blinking, leading to increased blink rates versus normal subjects [3]. Apraxia is a rare condition that may coincide with BL symptoms, involving failure of relaxation of the palpebral portion of the orbicularis oculi [4]. While some subjects experience brief symptoms, others experience prolonged symptoms that seriously affect quality of life. Within the US only, there are over 50,000 cases, with around 2,000 new diagnoses annually [5]. Despite the prevalence of BL, clinical evaluation is limited due to the subjective evaluation process and qualitative rating scales.

Physicians often evaluate patients in person or through recorded videos to observe muscle and eyelid activity in response to stimuli or while the patient is performing various activities [6]. The Jankovic Rating Scale (JRS) was the first scale specifically developed for BL [7]. The JRS is mostly qualitative and attempts to classify the intensity and frequency of spasms on a 5-point system [7], [8]. More recently the Blepharospasm Severity Rating Scale (BSRS) was introduced, to improve reliability and consistency [8]. The major limitation of both scales is the reliance on a human evaluator to count BL events and estimate the average duration of symptoms. This time-consuming and error-prone method leads to conflicting results based on individual evaluators [8]. Previously,

0018-9294 © 2020 IEEE. Personal use is permitted, but republication/redistribution requires IEEE permission. See https://www.ieee.org/publications/rights/index.html for more information.

electrophysiology has only been used in pathophysiology studies for tracking treatment progression with botulinum toxin [9]–[11], which utilized invasive fine needles to monitor specific muscles or even single muscle fibers.

Here, we introduce a flexible, hybrid, skin-like bioelectronics system (referred to as 'SKINTRONICS') that wirelessly detects non-invasive electrophysiological activities of the orbicularis oculi muscle. SKINTRONICS uses a set of ultrathin, nanomembrane electrodes and low-profile wearable circuit to measure the electrical signals around the eyes. Unlike conventional electrodes that require conductive gels and adhesives, the nanomembrane sensors offer a dry, highly comfortable lamination on the skin by matching mechanical properties with the epidermis. In addition, the miniaturized, soft wireless device that connects a set of electrodes provides an active, long-range (> 10 m) wireless detection of spasms via an Android-based tablet. The portable monitoring system implements a convolutional neural network (CNN) for a real-time, automated classification of key pathological symptoms and BL severity levels from the recorded data. We demonstrate the clinical feasibility of the SKINTRONICS with multiple patients, which captures a potential for wireless quantitative diagnostics of BL.

II. EXPERIMENTAL SECTION

A. Fabrication of Skintronics

SKINTRONICS has two major components including a flexible circuit and a set of nanomembrane electrodes. First, a thinfilm flexible circuit was patterned on a polydimethylsiloxane (PDMS)-coated Si wafer by following our prior work [12]–[14]. Details of the fabrication steps are provided in Supporting Note S1. After removing the completed circuit layers from the carrying wafer, functional chip components (Fig. S1 and Table S1) were integrated onto the exposed copper pads with a solder paste (SMDLTLFP10T5, Chip Quik). Finally, small magnets were attached to the electrode connection pads and circuit pads by using a silver conductive paint (Ted Pella). The assembled circuit was then encapsulated with a low-modulus elastomer mixture (Ecoflex Gel and Ecoflex 00–30, Smooth-On) to provide enough adhesion to the skin. Afterwards, a set of nanomembrane gold electrodes were fabricated via the combination of microfabrication [15] and material transfer printing [16]. Details of the fabrication steps appear in Supporting Note S2. Fabricated electrodes were then connected to the circuit via PDMS-insulated conductive film cables (HST-9805210, Elform) and small magnets. A small, rechargeable Li-polymer battery (capacity: 40 mAh, Digi-Key) was mounted on the circuit via conductive magnetic connection to power the SKINTRONICS.

B. Mechanical Study via Finite Element Analysis

Finite element analysis was conducted by using commercial software (Abaqus, Dassault Systemes) to design a highly flexible SKINTRONICS, while still offering a comfortable wear to subjects. The nanomembrane electrode that makes a direct skin contact (around the eyes) was designed to endure an excessive stretching and bending, while the electronic circuit that is laminated on a relatively flat, bony area (temple) was designed to

withstand a repetitive bending. The following material properties were used in the mechanics modeling study (E: Young's Modulus and ν : Poisson's Ratio): $E_{\rm Cu}=119$ GPa and $\nu_{\rm Cu}=0.34$ for copper; $E_{\rm PI}=2.5$ GPa and $\nu_{\rm PI}=0.34$ for polyimide [17], [18].

C. Experimental Mechanical Study

Biaxial stretching of fabricated electrodes was conducted on a programmable, cyclic stretcher (experimental setup in Fig. S2). The sample was held with four clamps that moved simultaneously for biaxial, cyclic stretching. A stepper motor, driven by a programmed circuit, was used to control stretching cycles. Thin copper wires (100 μm in diameter) were connected to the electrode to measure electrical resistance using a digital multimeter. For a mechanical bending test, electrodes were bent on the same testing platform with a pair of rigid holders, allowing a bending from 0 to 180°, with a radius of curvature of 500 μm . The electrical resistance was also measured during this test to find out any mechanical failure. Fabricated electronic circuits followed the same mechanical bending test to investigate the mechanical stability, while a wireless signal quality was measured to prove the functionality.

D. Study With Human Subjects

Thirteen symptomatic subjects, 5 males and 8 females, ages 25 to 65 participated in electrophysiological measurement based on the approved protocol (IRB #00024699) at Emory University. Subjects were provided an explanation for the study and had signed a consent form. Electrodes were placed above and below the eye, with the ground electrode placed on the forehead. The device was then placed on the temple before a battery was connected. Each subject was asked to follow prompts corresponding to an evaluation protocol while sitting. This protocol involved asking each subject to attempt a controlled blinking procedure of 5 blinks separated by 5 seconds. Afterwards, the subject was asked to forcibly close the eyes for 5 seconds at least five times. Then, the subject entered an observational period, where they looked ahead with minimal movement, attempting to blink naturally for 2 minutes. The protocol was designed to trigger BL symptoms so that the most severe symptoms can be observed. To detect BL symptoms, a clinical observer rated severity with the BSRS (example in Fig. S3) [8]. All of the studies were recorded with a digital video camera for additional review, if needed.

E. Data Acquisition via an Android Interface

All of the physiological data were monitored and recorded by an Android-tablet (Samsung Galaxy Tab) with a customdesigned application. Alternatively, the trained CNN was implemented to analyze the signal in 8-second segments. This allowed for displaying a summary of the rating results and relevant quantitative assessment immediately after the evaluation.

F. Analysis of Signal-to-Noise Ratio of the Recorded Data

Two minutes of time-series data were split into nonoverlapping 8-second segments (15 total). In this recording, a subject was asked to blink at regular intervals of one blink every 4 seconds. Calculation of signal-to-noise ratio (SNR) involves measurement of peak to peak amplitude from normal blinks and comparing it to the peak to peak magnitude of floor noise level using the following equation: $SNR_{dB} = 10\log_{10}[(A_{signal}/A_{noise})^2]$. The results were averaged over the number of windows in the recording and standard error of the mean was calculated.

G. Data Preprocessing

In order to preprocess the data without losing relevant information, a high-pass filter was used to remove DC offset and baseline drift. As shown in Fig. S4, 3rd-order high-pass Butterworth filter was applied at 0.2 Hz, 0.5 Hz, and 1.0 Hz. Classification accuracy was assessed by using a trained CNN based on manually labeled data from 13 subjects. The signals from the most conservative filter at 0.2 Hz, preserved the information required for classification, resulting in a classification accuracy of 99.1%. The 0.5 Hz filter performed with 94.9% accuracy and the 1.0 Hz filter performed the worst with 87.6% accuracy. Therefore, 0.2 Hz filter was used to achieve maximum accuracy.

H. Symptom Classification and Quantification

Digitized recordings from 13 subjects were manually labeled using four classes, including null (no activity), blink (normal or pathological), forced eye closure (spasm), and hemifacial spasm. Labels were applied by using a semantic segmentation where consecutive labels corresponded to consecutive electrophysiology data points in the time series. The labeling was based on simultaneously recorded camera footage of patients to determine the corresponding signals for each symptom. Classification was performed with a CNN, designed for semantic segmentation (network scheme shown in Fig. S5). Two minute recordings at a sampling rate of 250 Hz were segmented into overlapping 8-second samples, and the corresponding 4-class output labels were fed into the CNN algorithm. Each sample had 50% overlapping with the previous sample to analyze all events twice. This model calculated loss as the categorical cross-entropy and used the Adam optimizer with a fixed learning rate of 0.001. The CNN was trained by using a five-fold cross-validation paradigm, where data from all subjects were used. Here, non-randomized data were pooled together, and then split into 5 equal groups, which was to ensure less biased validation. The overall accuracy for the cross-validation was 99.1 \pm 2.8%, with only minor confusion relating to non-specific muscle contractions causing confusion in the 4-class model (Fig. S6). Supporting Note S3 provides details of analysis of out labels.

III. RESULTS AND DISCUSSION

A. Overview of Skintronics for Quantitative BL Detection

SKINTRONICS that combines a new class of technologies in nano-microfabrication, hard-soft materials integration, and soft material packaging enables a new way to quantify pathological symptoms and severity levels of BL. An overview of the system

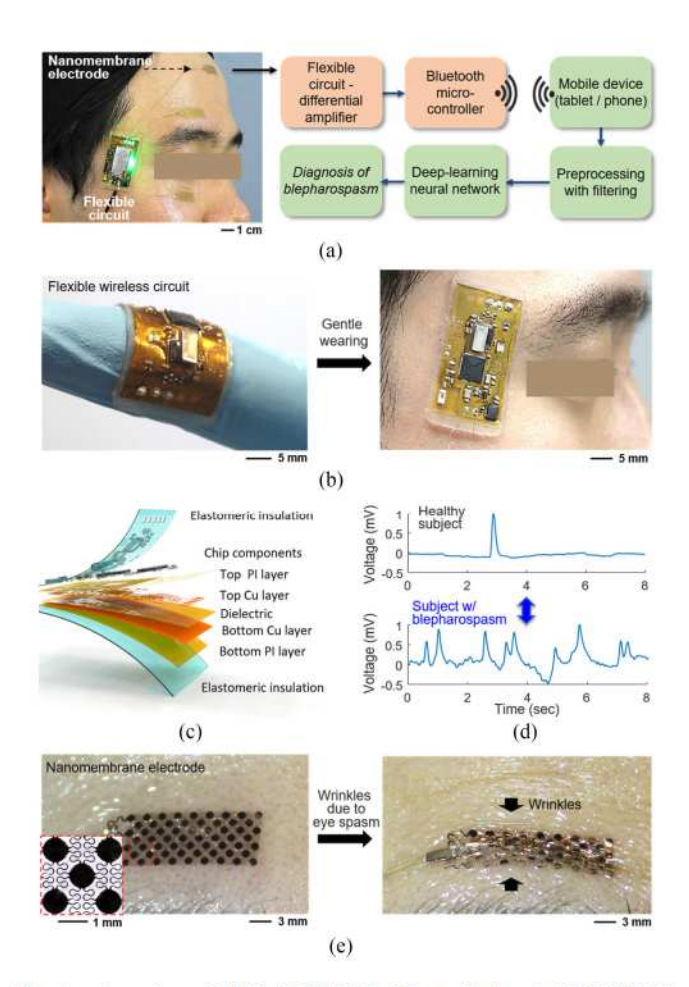


Fig. 1. Overview of SKINTRONICS for BL monitoring. (a) SKINTRONICS, including stretchable nanomembrane electrodes, placed above and below the eye of interest, with the 'ground' electrode on the forehead. The wireless, flexible circuit is placed on the side of head, near the temple. A flow chart (right) describes the data acquisition and data flow process. (b) Highly flexible, conformal SKINTRONICS (left) wrapped around a finger and close-up view of the device, gently mounted on temple, enabled by a soft elastomer (right). (c) Multi-layered structure of the wireless circuit. (d) Comparison of electrophysiological signals recorded on a healthy subject (top) and a subject with a BL symptom of pathological 'flutter' blinking (bottom). (e) Close-up view of a skin conformal nanomembrane electrode with an inset showing a mesh pattern (left) and contraction of forehead muscles showing flexibility and stretchability of the thin film electrode (right).

and data acquisition method is shown in Fig. 1(a), along with a flow chart describing key steps between data collection and BL evaluation. The electrophysiological data is transmitted via Bluetooth to a mobile device, where the data is analyzed in real-time to generate a quantitative assessment of symptoms as determined by machine learning techniques including CNN. A set of three nanomembrane electrodes is gently mounted on the skin around the eye and they are connected to a miniaturized soft flexible circuit via flexible film cables. Soft material packaging technique that embraces the electrodes, circuit, and cables offers a highly conformal, gentle wearing without the use of conductive gels and adhesives that typically cause skin breakdown [19], [20]. Adhesion properties of the membrane electronics have been thoroughly explored in prior work [19], [21], [22]. The device's mechanical flexibility and adhesion is

demonstrated in Fig. 1(b) via wrapping the circuit around a finger (left panel) and wearing it on the temple area (right panel). Encapsulation of the device with a low-modulus silicone elastomer (\sim 32 kPa) protects the sensitive electronics by distributing applied forces via deformation, which can avoid discomfort and artificial triggering of BL symptoms. This is the major advantage of SKINTRONICS by comparing with the invasive needle- or adhesive-based electrodes that can bias outcomes by stretching the orbicularis oculi muscle and triggering BL symptoms [23]. A schematic illustration in Fig. 1(c) captures the multi-layered structure of the wireless flexible circuit, including the ground plane, dielectric layer, metal interconnect, and integrated functional chip components. The circuit contains a Bluetooth system-on-chip with an analog front-end (ADS1292, Texas Instruments) for wireless recording of non-invasive electromyogram (EMG) signals on the orbicularis oculi muscle. The device is powered by a rechargeable, lithium-polymer battery (40 mAh) that can be simply mounted on and detached from the circuit via pairing of small magnets. Overall battery life of the device is approximately 5.1 hours from a full charge, which is longer than a single diagnostic trial. A representative EMG data (Fig. 1(d)), wirelessly measured by a custom-designed Android app, captures a clear difference between a healthy subject with normal blinking activity (top graph) and a patient with a BL symptom (bottom graph). The abnormal case shows more spontaneous fluctuations and frequent blinking. These fluctuations correspond to flutter blinking and spasm symptoms that affect a subject's quality of life. The excessive wrinkles on the very soft skin around the eyes are typically challenging to measure EMG signals with a conventional electrode that uses a thick metal and strong adhesive, which limits natural skin motions [24], [25]. Here, the newly developed, stretchable electrode with an open-mesh configuration offers a conformal lamination on the skin (Fig. 1e). The main contribution of this electrode is in active accommodation of repeated motions of skin compression and deformation without mechanical fracture during both spasms and normal activity.

B. Study of Mechanics and Reliability of SKINTRONICS

Design of a skin conformal and highly comfortable device requires mechanical stretchability and flexibility. SKINTRON-ICS has two major components of soft electrodes and wireless circuit where the electrode makes a direct contact to the highly stretchable and sensitive location around the eyes, while the circuit is mounted on a relatively flat surface (temple). Thus, we conducted a computational mechanics study (finite element analysis; FEA) to design a highly stretchable electrode to avoid any unwanted mechanical fracture, while offering a flexible circuit to provide a comfortable wear. FEA result in Fig. 2(a), top shows a unit cell of the electrode with an applied 40% biaxial strain, resulting in maximum principle strains below 1% (fracture limit of Au: 1%) [26]. Experimental stretching of the electrode (Fig. 2(a), bottom) confirms the ability of 40% stretching and return without damaging the electrode. Additionally, FEA estimates the effect of mechanical bending of 180° at a $500-\mu m$ radius of curvature (Fig. 2(b), top), which also shows less than

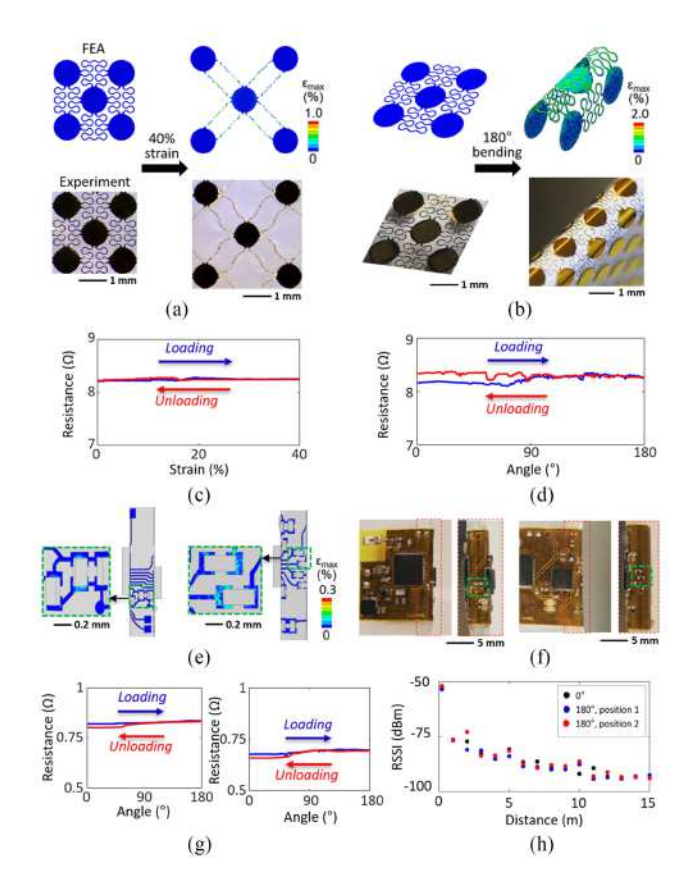


Fig. 2. Mechanical behavior of the device via computational modeling and experimental validation. (a) FEA result (top) of the electrode subunit, showing 40% stretchability with excellent correspondence to the experimental case (bottom), with strains maintained under 1%. (b) FEA data (top) of bending of 180°, along with experimental validation (bottom). (c) Result of an electrical resistance measurement corresponding to 40% stretching and relaxation of electrode, showing negligible change. (d) Cyclic bending of the device with electrical resistance measurement, also showing negligible change. (e) FEA results at two locations simulating strain of the interconnects during 180° bending results in strain below 0.3%. (f) Photos of the data acquisition device bending at 180° in two separate locations, with (g) loading and unloading curves plotting electrical resistance at two interconnect locations showing minimal change. (h) RSSI measurements showing consistency with device at 180° bend versus device in unbent configuration.

2% of maximum principle strains. Experimental bending the electrode (Fig. 2(b), bottom) validates mechanical reliability without fracture during multiple bending over small curvatures. To quantify the structural integrity of the fabricated electrode upon stretching (40%) and bending (180°), a cyclic loading test measures the change of electrical resistance (Fig. 2(c) and 2(d)), which shows a negligible effect on the mechanical deformation. In addition, FEA study is performed to simulate 180° bending of a flexible circuit, consisting of thin-film metal interconnects and rigid chip components. Mechanical bending at two locations with radius of curvature of 1.5 mm shows a minimized change of maximum principle strain of less than 0.3%, smaller than the fracture limit of 5% [15] (Fig. 2(e)). An experimental test in Fig. 2(f) validates the mechanical flexibility of the fabricated electronics on both locations without fracture. Electrical resistance between interconnects at these locations are monitored during the cyclic bending to investigate device

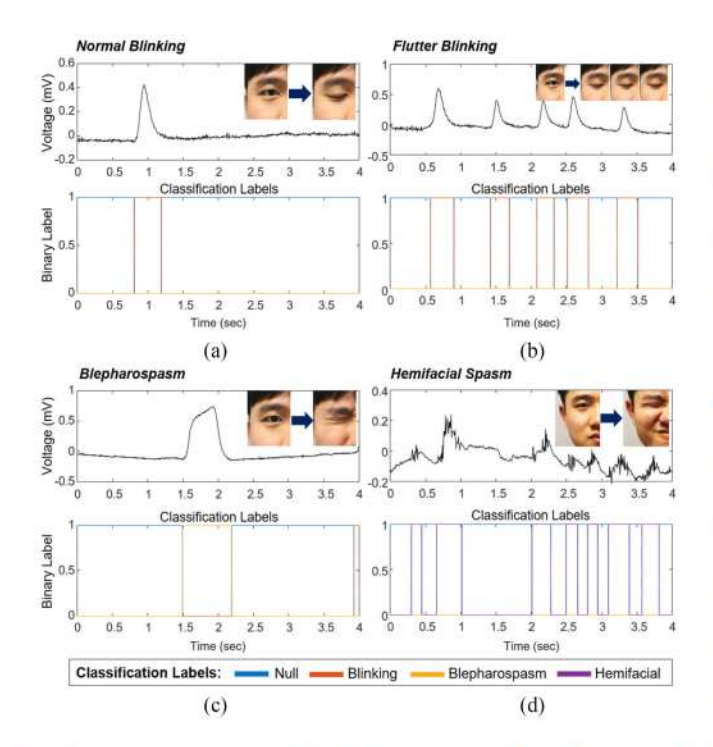


Fig. 3. Data samples and labels for detection of BL symptoms. (a) Electrophysiological signals (top) of normal blink from asymptomatic subject, along with inset demonstrating blink action, and labels (bottom) from CNN classification showing precise semantic segmentation, with legend inset. (b) Signals (top) of a pathological 'flutter' blinking scheme of blepharospasm subject, along with inset demonstrating multiple consecutive blinks, and labels (bottom) from CNN. (c) Signals of a BL symptom, forced eye closure, with an inset showing forced eye closure action, and labels (bottom) showing CNN semantic segmentation. (d) High frequency signals (top) of hemifacial spasms from a subject, with inset demonstrating forced eye closure with hemifacial involvement, and labels (bottom) showing CNN semantic segmentation precisely labeling each event.

stability (Fig. 2(g)), which shows a minimal fluctuation of resistance ($<0.1~\Omega$). Additionally, a wireless received signal strength indication (RSSI) is monitored during device bending at both locations (Fig. 2(h)), which demonstrates that the antenna power and wireless connection is consistent despite bending upto 15 m. Overall, the presented set of computational and experimental studies clearly capture the mechanical reliability of the SKINTRONICS and stable wireless data acquisition, showing a potential for a comfortable, long-term wear on the skin for quantitative BL diagnosis.

C. Analysis of EMG Signals for Labeling and Classification of BL Symptoms

To quantitatively measure and distinguish multiple BL features, time-domain data were segmented to determine frequency and duration of symptoms. Fig. 3 summarizes a representative set of data that capture normal blinking, flutter blinking, forced eye closure (BL), and hemifacial spasm. Fig. 3(a) shows a normal blink signal with an inset photo demonstrating normal eye closure and classification labels (bottom graph) that clearly captures either null signals or blinking. It should be noted that blinks in isolation are not necessarily symptomatic of BL, thus

it is required to detect multiple events (Fig. 3(b)) that accurately presents length and location of each blink event. Unlike normal blinking, forced eye closure (BL in Fig. 3(c)) shows longer a plateaued signal (top graph), along with a different label than blinking (bottom). Hemifacial spasm is a related disorder that may manifest as BL-like symptoms (Fig. 3(d)), where one side of the face experiences sudden involuntary muscular contractions at irregular intervals. This spasm results in high-frequency signals on the channels and are labeled as such (bottom graph). We collected EMG data from 13 human subjects to enable accurate classification of all symptoms. Among them, five subject data were used to train a CNN (details in Fig. S5). For the CNN architecture, semantic segmentation was used that incorporated inception-type convolutional units [27], along with residual connections for purposes of segmentation [28]. The segmentation process is important because the precise duration of symptoms are required to understand disease progression. Overall, the CNN is preferred, compared to the conventional feature extraction and classification methods due to greater precision in labeling boundaries. In addition, CNN method allows for efficient training on small-labeled datasets with high accuracies. The trained models can be readily implemented in a mobile device for a real-time data acquisition. Using 5-fold cross-validation across a dataset of 13 human subjects, the CNN achieved an accuracy of 99.1 \pm 2.8% with the preprocessing method.

D. Validation of the Device Performance

To validate the performance of SKINTRONICS, we measured the targeted EMG data along with a commercial wireless device (BioRadio, Great Lakes NeuroTechnologies), mounted on the skin together (Fig. 4). A subject in Fig. 4(a) has both devices, which clearly captures the low-profile, unobtrusive arrangement of SKINTRONICS. The first set of testing (Fig. 4(b)) measures random blinking at varying frequencies. Overall, two devices show indistinguishable signal features even though the commercial one (SNR: 25.4 ± 4.3 dB) has slightly higher signal than the SKINTRONICS (SNR: 22.4 ± 2.1 dB). However, the rigid electrode with the adhesive tape on the skin shows delamination after 1 hour of recording (Fig. 4(c)), which can be explained by the significant skin flexion during the test. The increased delamination results in a poor contact with skin, which causes decreased SNR (drop of 6.2 dB) of the conventional system (Fig. 4(d)). On the other hand, the SNR of the SKINTRON-ICS remains consistent. In addition, the SKINTRONICS has minimized motion artifacts, compared to the BioRadio system (Fig. 4(e) and 4(f)). The subject intentionally generated head movements, turning up and down (Fig. 4(e)) and turning left and right (Fig. 4(f)). Note that the data in this comparison have been processed by using a 3rd-order Butterworth high-pass filter with a 2-Hz cutoff in order to match the baselines and adequately compare SNR between two devices. The measured data show that the SKINTRONICS has a better performance due to minimal wire movement and electrode dragging effects with a gel and tape. Overall, the validation study shows a great potential of SKINTRONICS for a continuous, long-term recording of BL symptoms with the miniaturized, portable system.

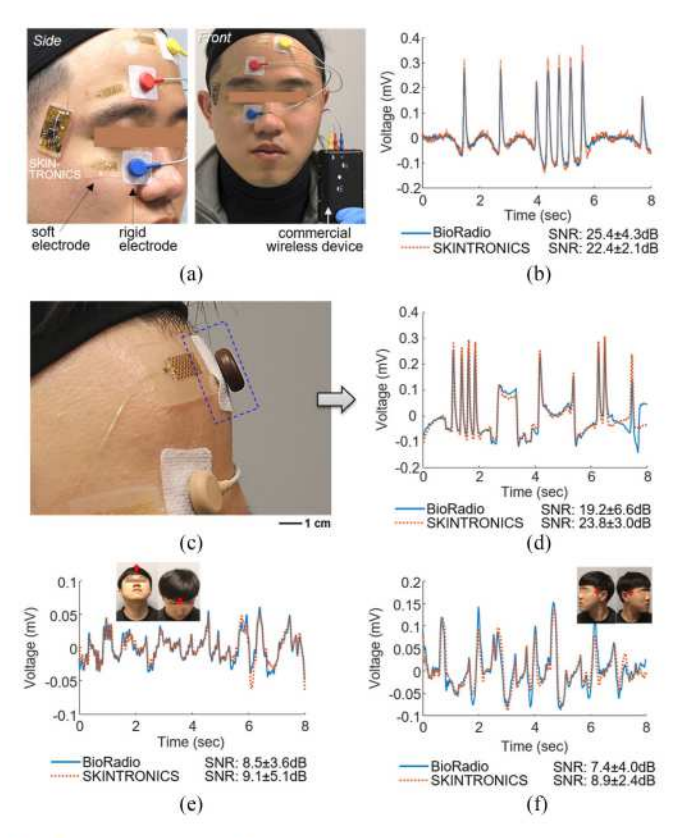


Fig. 4. Comparison of device performance between SKINTRONICS and a commercial wireless system. (a) Experimental setup comparing the device form factor between SKINTRONICS with unobtrusive arrangement and BioRadio data acquisition device and rigid electrodes. (b) Simultaneous recording of 'flutter' blinking symptoms, showing strong correlation, with similar SNR values. (c) Photo of both electrodes that shows delamination of the conventional electrode after 1 hour of use. (d) Simultaneous recordings and SNR analysis from both devices after 1 hour of use, showing a decrease in sensitivity from the conventional electrode system. (e) Graph of noise level of up-down head movements (inset) with normal activity (no blinks or spasms), with SNR analysis. (f) Graph of noise level of left-right head swivel movements (inset) with normal activity, with SNR analysis.

E. Quantitative Digital Scaling of BL and Comparison to Human Ratings

Classification of BL electrophysiological data was performed using a CNN. First, the data were preprocessed using a 0.2 Hz high-pass Butterworth filter, order of 3, and the features are rescaled between 0 and 1, before being fed into the CNN for training. A flow chart summarizing this procedure is shown in Fig. 5(a). The architecture of the CNN is provided in Fig. S3. The paradigm used here is called semantic segmentation, designed to output labels for each input data point. These labels are more useful for quantitative analysis, where the frequency and duration of symptoms are used to generate severity ratings for each subject according to the BSRS rating scale. The analysis of the output labels is detailed in Supporting Information Note S3. This analysis results in quantitative frequency and duration information (Table S2), which are more useful to understand disease progression versus human observation or video recording. The summarized data set in Fig. S6 shows samples of data exhibiting each symptom, along with correct labeling, and an

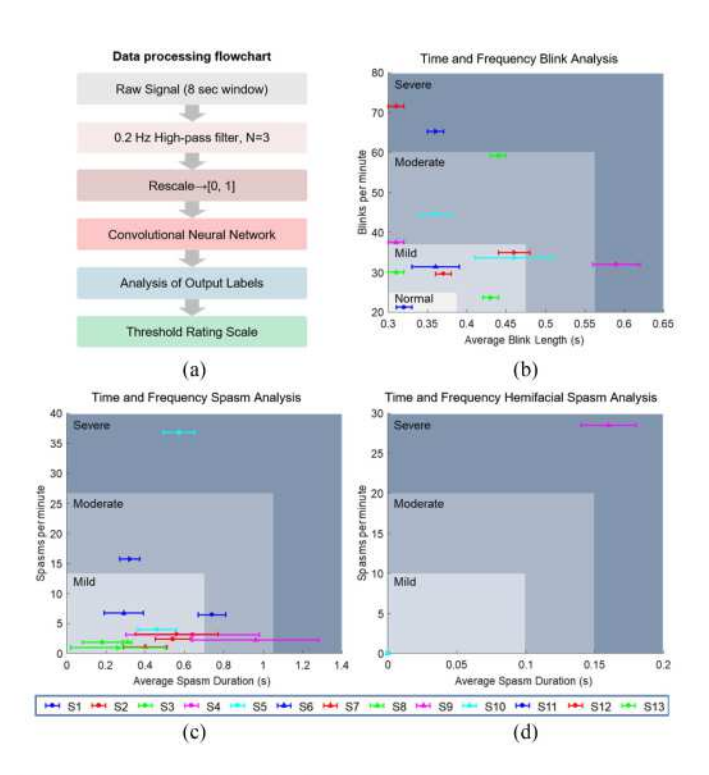


Fig. 5. Digital scaling of BL symptoms from 13 patients. (a) A flowchart with an overview of data processing and classification scheme of electrophysiological data from SKINTRONICS. Quantitative evaluation of (b) blink statistics from 13 patients including blink rate and average blink length, (c) spasm rate and duration, and (d) hemifacial spasm rate and duration. For each symptom, four colors represent severity levels including 'normal', 'mild', 'moderate' and 'severe', accounting for frequency and duration.

TABLE I

COMPARISON OF SEVERITY LEVELS BETWEEN DIGITAL ASSESSMENT FROM SKINTRONICS AND MANUAL CLINICAL EVALUATION [8]

| Subject ID | Eye Spasms | | Average Duration of Long Eye Spasms | | Frequency of Normal Blinks | | Frequency of Long Eye Spasms | |
|---------------|------------|---------|--|---------|-------------------------------|---------|------------------------------------|---------|
| | Manual | Digital | Manual | Digital | Manual | Digital | Manual | Digital |
| S1 | 1 | 1 | 0 | 0 | 2 | 2 | 0 | 0 |
| S2 | 0 | 1 | 0 | 0 | 1 | 2 | 0 | 0 |
| S3 | 1 | 1 | 0 | 0 | 2 | 3 | 0 | 0 |
| S4 | 1 | 1 | 0 | O | 2 | 2 | 0 | 0 |
| S5 | 1 | 1 | 0 | O | 3 | 3 | 0 | 0 |
| S6 | 0 | 1 | 0 | O | 1 | 2 | 0 | 0 |
| S7 | 0 | 1 | 0 | 0 | 3 | 3 | 0 | 0 |
| S8 | 1, 2 | 1 | 3 | 0 | 2 | 2 | 1 | 0 |
| S9 | 1, 2 | 1 | 1 | 0 | 2 | 3 | 0 | 0 |
| S10 | 1 | 1 | 0 | 1 | 2 | 3 | 0 | 1 |
| S11 | 1 | 1 | 0 | 0 | 3 | 3 | 0 | 0 |
| S12 | 1 | 1 | 0 | 0 | 2 | 2 | 0 | 0 |
| S13 | 1 | 1 | 0 | 0 | 2 | 2 | 0 | 0 |

overall confusion matrix indicating the high precision of this system. The quantitative analysis is then mapped to BSRS rating scale using the relevant sections that use quantitative data and compared with human ratings. These results are summarized in Table I, showing a strong correspondence to the human

ratings. We believe that the digital scaling from the machine analysis offers more accurate, objective measure, while manual rating has a possible human error shown as discrepancy in the result. The quantitative analysis is represented in Fig. 5(b-d) that capture symptom severity levels in terms of frequency (events per minute) and duration (in seconds). The three major recorded symptoms among 13 subjects, including pathological flutter blinking (Fig. 5(b)), forced eye closure (Fig. 5(c)), and hemifacial spasm, detected in only one subject (Fig. 5(d)). These quantitative results show the variation in symptoms with greater nuance than is possible with a multi-point rating system used by a human rating. Overall, the result of digital scaling of EMG data clearly shows the advantage of SKINTRONICS in objective diagnostics of BL symptoms and severity levels without any human error and time-consuming manual assessment. This study will be further extended to allow an on-site, real-time evaluation and diagnosis of BL symptoms. During the patient study, we found that a single-channel EMG system is likely to pick up interference from other muscles that are not specifically targeted. Thus, our future work aims to tackle the isolation of specific muscle involvement with a greater number of test subjects for more precise diagnosis of BL.

IV. CONCLUSION

We have demonstrated the feasibility of wearable SKIN-TRONICS for wireless quantitative assessment of BL. The skin-friendly system enables a high-quality, real-time recording of electrophysiological signals from the contoured and dimpled skin with enhanced SNR compared to a commercial system due to minimized motion artifacts. This all-in-one wearable solution will allow physicians to quickly generate quantitative data for accurate BL assessments and disease progression by eliminating subjective and manual diagnosis. When consider four symptoms, including null (no activity), blink, force spasm, and hemifacial spasm, the overall accuracy for the cross-validation is 99.1 \pm 2.8%, with only minor confusion relating to nonspecific muscle contractions. Collectively, the proposed system shows significant potential as a clinical diagnostic tool with improved ergonomics and comfortable, long-term wearability. Future work will focus on a new testing setup with multi-channel electrophysiological recording, which would determine spasmrelated origin, resulting in 100% classification accuracy.

REFERENCES

- G. Defazio et al., "Blepharospasm 40 years later," Movement Disorders, vol. 32, no. 4, pp. 498–509, 2017.
- [2] M. Hallett, "Blepharospasm: Recent advances," Neurology, vol. 59, no. 9, pp. 1306–1312, 2002.
- [3] A. R. Bentivoglio et al., "Analysis of blink rate in patients with ble-pharospasm," Movement Disorders: Official J. Movement Disorder Soc., vol. 21, no. 8, pp. 1225–1229, 2006.
- [4] P. Lamberti et al., "Frequency of Apraxia of eyelid opening in the general population and in patients with extrapyramidal disorders," Neurological Sci., vol. 23, no. 2, pp. s81–s82, 2002.

- [5] W. H. Adams et al., "The evaluation of light sensitivity in benign essential blepharospasm," Amer. J. Ophthalmol., vol. 142, no. 1, pp. 82–87. e8, 2006.
- [6] E. D. Louis, B. Ford, and B. Bismuth, "Reliability between two observers using a protocol for diagnosing essential tremor," *Movement Disorders: Official J. Movement Disorder Soc.*, vol. 13, no. 2, pp. 287–293, 1998.
- [7] J. Jankovic and J. Orman, "Botulinum A toxin for cranial-cervical dystonia: A double-blind, placebo-controlled study," *Neurology*, vol. 37, no. 4, pp. 616–616, 1987.
- [8] G. Defazio et al., "Development and validation of a clinical scale for rating the severity of blepharospasm," Movement Disorders, vol. 30, no. 4, pp. 525–530, 2015.
- [9] D. Sanders, E. W. Massey, and E. Buckley, "Botulinum toxin for blepharospasm: Single-fiber EMG studies," *Neurology*, vol. 36, no. 4, pp. 545–547, 1986.
- [10] A. Berardelli et al., "Pathophysiology of blepharospasm and oromandibular dystonia," Brain, vol. 108, no. 3, pp. 593–608, 1985.
- [11] J. D. Rollnik et al., "Low-dose treatment of cervical dystonia, ble-pharospasm and facial hemispasm with albumin-diluted botulinum toxin type A under EMG guidance," Eur. Neurol., vol. 43, no. 1, pp. 9–12, 2000.
- [12] Y. S. Kim et al., "Scalable manufacturing of solderable and stretchable physiologic sensing systems," Adv. Mater., vol. 29, no. 39, 2017, Art. no. 1701312.
- [13] J. A. Fan et al., "Fractal design concepts for stretchable electronics," Nature Commun., vol. 5, 2014, Art. no. 3266.
- [14] W. H. Yeo et al., "Multifunctional epidermal electronics printed directly onto the skin," Adv. Mater., vol. 25, no. 20, pp. 2773–2778, 2013.
- [15] Y. Lee et al., "Wireless, intraoral hybrid electronics for real-time quantification of sodium intake toward hypertension management," Proc. Nat. Acad. Sci., vol. 115, no. 21, 2018, Art. no. 5377.
- [16] Y.-S. Kim et al., "All-in-one, wireless, stretchable hybrid electronics for smart, connected, and ambulatory physiological monitoring," Adv. Sci., vol. 6, no. 17, 2019, Art. no. 1900939.
- [17] Y. Zhang et al., "Frequency recognition in SSVEP-based BCI using multiset canonical correlation analysis," Int. J. Neural Syst., vol. 24, no. 4, Jun. 2014, Art. no. 1450013.
- [18] R. Xu et al., "Fabric-based stretchable electronics with mechanically optimized designs and prestrained composite substrates," Extreme Mechanics Lett., vol. 1, pp. 120–126, 2014.
- [19] Y. S. Kim et al., "All-in-one, wireless, stretchable hybrid electronics for smart, connected, and ambulatory physiological monitoring," Adv. Sci., vol. 6, no. 17, 2019, Art. no. 1900939.
- [20] S. Mishra et al., "Soft, conformal bioelectronics for a wireless humanwheelchair interface," Biosensors Bioelectronics, vol. 91, pp. 796–803, 2017.
- [21] Y. T. Kwon et al., "Soft material-enabled, active wireless, thin-film bioelectronics for quantitative diagnostics of cervical dystonia," Adv. Mater. Technologies, vol. 4, no. 10, 2019, Art. no. 1900458.
- [22] S. Kwon et al., "Skin-conformal, soft material-enabled bioelectronic system with minimized motion artifacts for reliable health and performance monitoring of athletes," Biosensors Bioelectronics, vol. 1512020, Art. no. 111981.
- [23] J. Obeso, J. Artieda, and C. Marsden, "Stretch reflex blepharospasm," Neurology, vol. 35, no. 9, pp. 1378–1378, 1985.
- [24] H. R. Lim et al., "Advanced soft materials, sensor integrations, and applications of wearable flexible hybrid electronics in healthcare, energy, and environment," Adv. Mater., vol. 32, no. 15, Apr. 2020, Art. no. 1901924.
- [25] R. Herbert et al., "Soft material-enabled, flexible hybrid electronics for medicine, healthcare, and human-machine interfaces," *Materials*, vol. 11, no. 2, p. 187, 2018.
- [26] J. W. Jeong et al., "Materials and optimized designs for human-machine interfaces via epidermal electronics," Adv. Mater., vol. 25, no. 47, pp. 6839– 6846, 2013.
- [27] C. Szegedy et al., "Going deeper with convolutions," in Proc. IEEE Conf. Comput. Vision Pattern Recognit., 2015, pp. 1–9.
- [28] J. Long, E. Shelhamer, and T. Darrell, "Fully convolutional networks for semantic segmentation," in Proc. IEEE Conf. Comput. Vision Pattern Recognit., 2015, pp. 3431–3440.

Supporting Information

Soft Nanomembrane Sensors and Flexible Hybrid Bioelectronics for Wireless Quantification of Blepharospasm

Musa Mahmood, Shinjae Kwon, Gamze Kilic Berkmen, Yun-Soung Kim, Laura Scorr, H. A. Jinnah, and Woon-Hong Yeo*

M. Mahmood, S. Kwon, Dr. Y. Kim, Prof. W.-H. Yeo

George W. Woodruff School of Mechanical Engineering, Institute for Electronics and Nanotechnology, Georgia Institute of Technology, Atlanta, GA 30332, USA

Dr. G. K. Berkmen, Dr. L. Scorr, Dr. H. A. Jinnah

Departments of Neurology and Human Genetics, School of Medicine, Emory University, GA 30322, USA

Prof. W.-H. Yeo

Wallace H. Coulter Department of Biomedical Engineering, Neural Engineering Center, Parker H. Petit Institute for Bioengineering and Biosciences, Center for Flexible and Wearable Electronics Advanced Research, Institute for Materials, Institute for Robotics and Intelligent Machines, Georgia Institute of Technology, Atlanta, GA 30332, USA

E-mail: whyeo@gatech.edu (W.-H. Yeo)

Section S1. Fabrication steps of a flexible circuit.

There are two major processes, including many steps as shown below:

- a) Microfabrication of the thin-film circuit boards
 - 1. Spincoat PDMS on a cleaned silicon wafer at 4000 rpm for 30 sec.
 - 2. Cure the PDMS-coated wafer on a 150 °C hot plate for 5 min.
 - 3. Perform oxygen plasma treatment to render the PDMS hydrophilic.
 - Spincoat polyimide at 2000 rpm for 1 min and bake in a vacuum oven at 250 °C for 3 hr including ramping steps.
 - 5. Sputter 500 nm copper for the first metal layer.
 - 6. Spincoat photoresist (PR, Microposit SC1813, MicroChem) at 3000 rpm for 30 sec and bake it on a 100 °C hot plate for 3 min.
 - 7. Expose UV with the first metal pattern (ground) using a mask aligner (MA6, Karl Suss).
 - 8. Develop the exposed photoresist with developer (MF-319, MicroChem).
 - 9. Etch exposed copper with copper etchant (APS-100, diluted 1:1 with DI water, Transene) and strip photoresist.
 - 10. Spincoat polyimide at 1000 rpm for 1 min and soft bake on a hot plate at 100°C for 10 min.
 - 11. Spincoat polyimide at 1000 rpm for 1 min and soft bake on a hot plate at 100°C for 5 min.
 - 12. Hard bake in a vacuum oven at 250 °C for 3 hr including ramping steps.
 - 13. Spincoat photoresist (AZP4620, Integrated Micro Materials) at 900 rpm for 30 sec and bake it on a 90 °C hot plate for 5 min.
 - 14. Expose UV with the first via pattern using a mask aligner (MA6).
 - Develop the exposed photoresist with developer (AZ-400K, diluted with four parts of DI water, Integrated Micro Materials).
 - Oxygen plasma etch exposed PI using reactive ion etching (Plasma-Therm) and strip photoresist.
 - 17. Sputter 1.5 μm copper for the second metal layer.
 - 18. Spincoat photoresist (AZP4620) at 2000 rpm for 30 sec and bake it on a 90 °C hot plate for 4 min.
 - 19. Expose UV on the second metal pattern using a mask aligner (MA6).
 - Develop the exposed photoresist with developer (AZ-400K, diluted with four parts of DI water).
 - Etch exposed copper with copper etchant (APS-100, diluted 1:1 with DI water) and strip
 photoresist.

- 22. Spincoat polyimide at 2000 rpm for 1 min and soft bake on a hot plate at 100°C for 5 min.
- 23. Hard bake in a vacuum oven at 250 °C for 3 hr including ramping steps.
- 24. Spincoat photoresist (AZP4620) at 2000 rpm for 30 sec and bake it on a 90 °C hot plate for 4 min.
- 25. Expose UV with the solder pad exposure pattern using a mask aligner (MA6).
- Develop the exposed photoresist with developer (AZ-400K, diluted with four parts of DI water).
- Oxygen plasma etch exposed PI using reactive ion etching (Plasma-Therm) and strip photoresist.
- 28. Completed circuits are peeled-off from the PDMS wafer.
- b) Assembly of a flexible circuit board using reflow soldering
 - 1. Openings of the stainless steel stencil is aligned to the exposed copper pads.
 - Solder paste is dispensed onto the stencil is dragged across the stencil with a flat plastic plate.
 - 3. Chip components are placed on the board.
 - 4. Using a programmable hot plate, the components are reflow soldered by ramping the hot plate from 100 °C to 170 °C at an increment of 10 °C with a 1 min dwell period at each temperature.
 - 5. Magnetic power connectors are soldered on the board.
 - Soldered board is rinsed with acetone and isopropyl alcohol and dried with a stream of nitrogen.
 - 7. Magnets are attached on the contact pads with small amount of silver paint.
 - 8. The board is detached from the glass slide and is attached to a thin layer of elastomer.

Section S2. Fabrication of skin-conformal nanomembrane electrodes.

Detailed procedures involved in thin-film electrode fabrication are as follows:

- a) Microfabrication process
 - 1. Spincoat PDMS on a cleaned silicon wafer at 4000 rpm for 30 sec.
 - 2. Cure the PDMS-coated wafer on a 150 °C hot plate for 5 min.
 - 3. Perform oxygen plasma treatment to render the PDMS hydrophilic.
 - Spincoat polyimide (PI, HD MicroSystems) at 2000 rpm for 1 min and bake in a vacuum oven at 250 °C for 3 hr including ramping steps.
 - 5. Sputter 5/200 nm of Cr/Au on top of PI.
 - 6. Spincoat photoresist (PR, Microposit SC1813, MicroChem) at 3000 rpm for 30 sec and bake it on a 100 °C hot plate for 3 min.
 - 7. Expose UV on the PR using a mask aligner (MA6, Karl Suss).
 - 8. Develop the exposed photoresist with developer (MF-319, MicroChem).
 - 9. Etch exposed Au with Au etchant (GE-8110, Transene).
 - 10. Etch exposed Cr with Cr etchant (Chrome Mask Etchant 9030, Transene).
 - 11. Oxygen plasma etch exposed PI using reactive ion etching (Plasma-Therm) and strip photoresist.
- b) Assembly with a thin film cable
 - Tape PVA film (polyvinyl alcohol, Haining Sprutop Chemical Tech, China) on a flat glass slide.
 - 2. Spincoat Ecoflex Gel at 1000 RPM for 1 min, and cure it on a hot plate at 50°C for 10 min.
 - 3. Treat the Ecoflex/PVA substrate with oxygen plasma.
 - 4. Pick up the electrode from wafer with water-soluble tape.
 - Transfer the electrode on the Ecoflex/PVA substrate, and gently wash off the water-soluble tape under flowing DI water.
 - One end of conductive film cable (HST-9805210, Elform) is attached on the contact pad of the electrode with small amount of silver paint.
 - Magnet is attached on the other end of the conductive film cable with small amount of silver paint.
 - 8. Insulate the exposed area of conductive film cable with PDMS.

Section S3. Analysis of output labels toward symptom quantification.

Towards quantifying and establishing ratings for the CNN-labeled and segmented data, the labels are maximized (see Figure S4), and anomalous labels are set to null.

For example, on the rare occasion that a sequence is labeled symptomatic for shorter than 0.1 seconds, the labeling is assumed to be incorrect and is removed. Then the following metrics are extracted from the labels: average blink duration in seconds, blink rate (minute⁻¹), average eye spasm duration (seconds), eye spasm rate (minute⁻¹), average hemifacial spasm duration (seconds), and hemifacial spasm rate (minute⁻¹).

These metrics can then be used to correspond with rating scales like the Blepharospasm Severity Rating Scale (reference scale shown in Figure S3) (1).

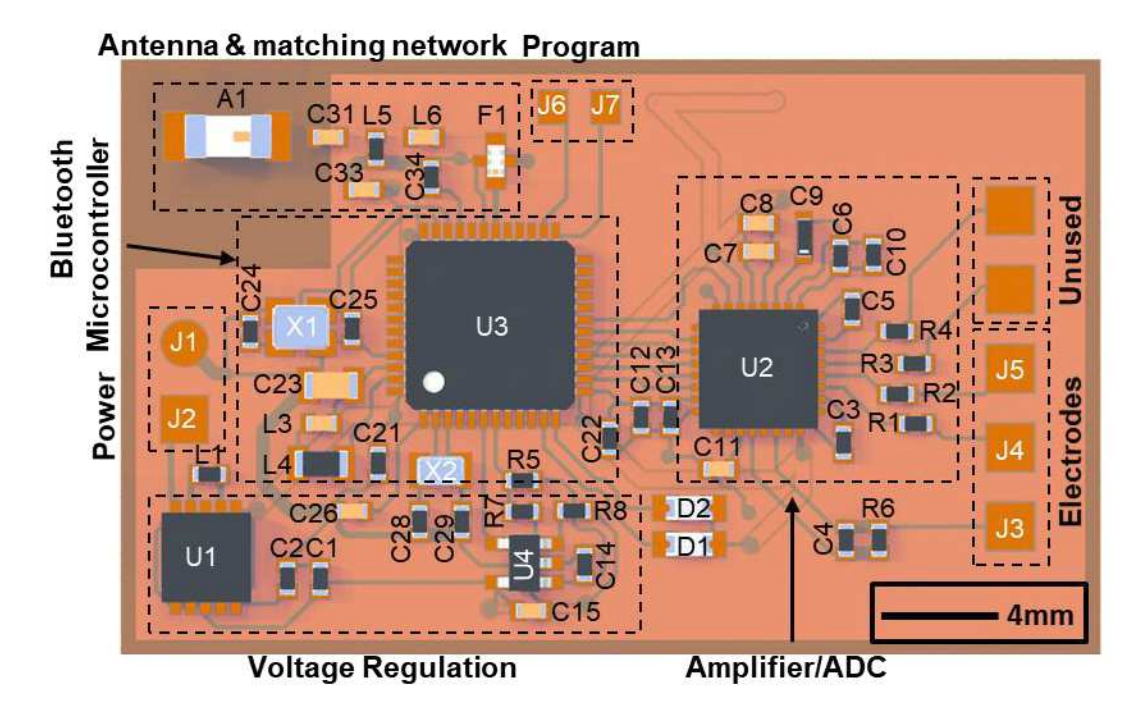


Figure S1. Circuit design. Top-view illustration of SKINTRONICS data acquisition circuitry, with highlighted functional blocks. A detailed list of the surface mount components can be found in Table S2. Dimensions of the circuit are 32.3 x 20.5mm.

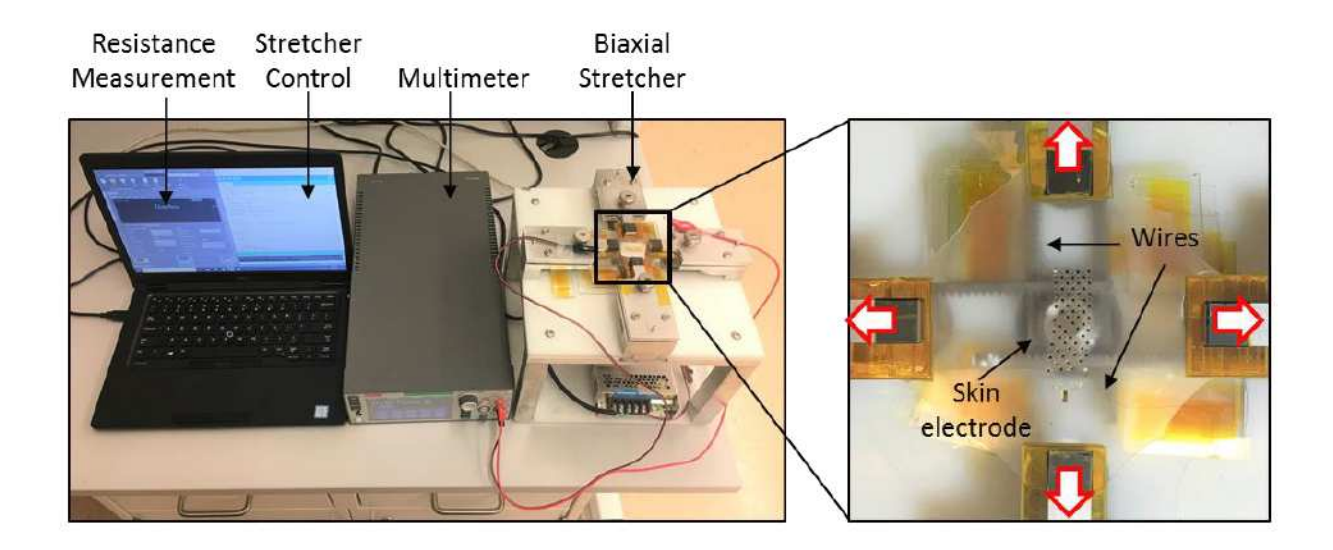


Figure S2. Mechanical testing setup. The left panel shows the setup with a multimeter and laptop for control for the biaxial stretcher. The right panel shows a close-up of the electrode in a biaxial stretch, with the wires attached for electrical resistance measurement.

| A1: EYE SPASMS | Types of Spasms (select one choice from each of the 3 options) | | | | | | |
|---|--|---|--|---|---|---|--|
| A spasm is defined as a complete or partial eyelid narrowing with accompanying evidence of activation of additional facial muscles beyond the pre-tarsal orbicularis oculi muscles. Activity of | Brief (<3 sec) spasms with complete rim closure | | Long (>3 sec) spasms with partial rim closure | | Long (>3 sec) spasms with complete rim closure | | |
| these additional muscles is expressed by additional movements of other regions of the face during eye closures, such as downward movement | None | 0 | None | 0 | None | 0 | |
| of the eyebrow or upward movement of the lower eye region, often leading to a squinting appearance. Spasms may be short or long, partial or complete, tonic or dynamic. | At least one | 1 | At least one | 2 | At least one | 3 | |

| A4: AVERAGE DURATION OF LONG EYE SPASMS | Duration | |
|---|-----------------|---|
| If the participant has long eye spasms (>3 sec in duration), please estimate the average duration of | No long spasms | 0 |
| nese spasms. This estimate should come from the 2-minute recording at the end of the video rotocol, when the patient is at rest with eyes open. | 3 - 4 seconds | 1 |
| | 4.1 - 5 seconds | 2 |
| | > 5 seconds | 3 |

| B1: FREQUENCY OF NORMAL BLINKS PLUS BRIEF EYE SPASMS | Frequency | | |
|---|---------------------|---|--|
| Please estimate the frequency of normal blinks combined with brief spasms per minute. For this | No blinks or spasms | 0 | |
| ate, blinks and brief spasms are combined. This estimate should come from the 2-minute ding at the end of the video protocol, when the patient is at rest with eyes open. | 1 - 18 (per min) | 1 | |
| | 19 - 32 (per min) | 2 | |
| | > 32 (per min) | 3 | |

| B2: FREQUENCY OF LONG EYE SPASMS WITH COMPLETE RIM CLOSURE | Frequency | |
|---|-------------------|---|
| spasms per minute. This estimate should come from the 2-minute recording at the end of the video protocol, when the patient is at rest with eyes open. The total number of these spasms should be | No long spasms | 0 |
| | 1 - 3 (per min) | 1 |
| divided by 2 to get the frequency/minute. | 3.1 - 7 (per min) | 2 |
| | > 7 (per min) | 3 |

Figure S3. BL severity rating scale used at clinics. Selected relevant sections of rating scale developed by Defazio et al.(1), including rating scale for eye spasms and blinks.

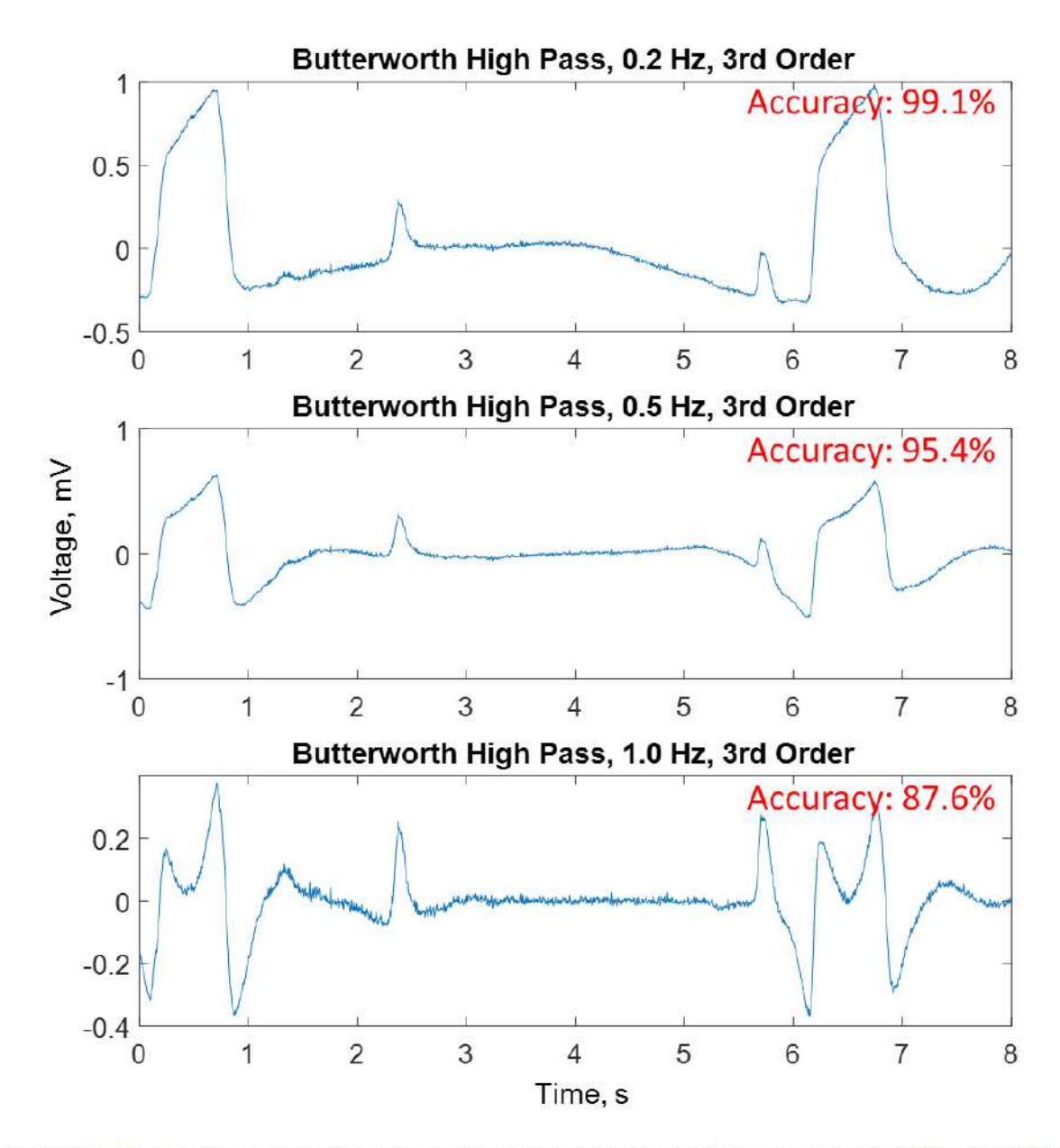


Figure S4. BL data preprocessing. Comparison of signals after high-pass Butterworth filtering at different cutoff frequencies. At 0.2 Hz, the spasm symptoms are least distorted and result in the highest accuracies when classified with the convolutional neural network.

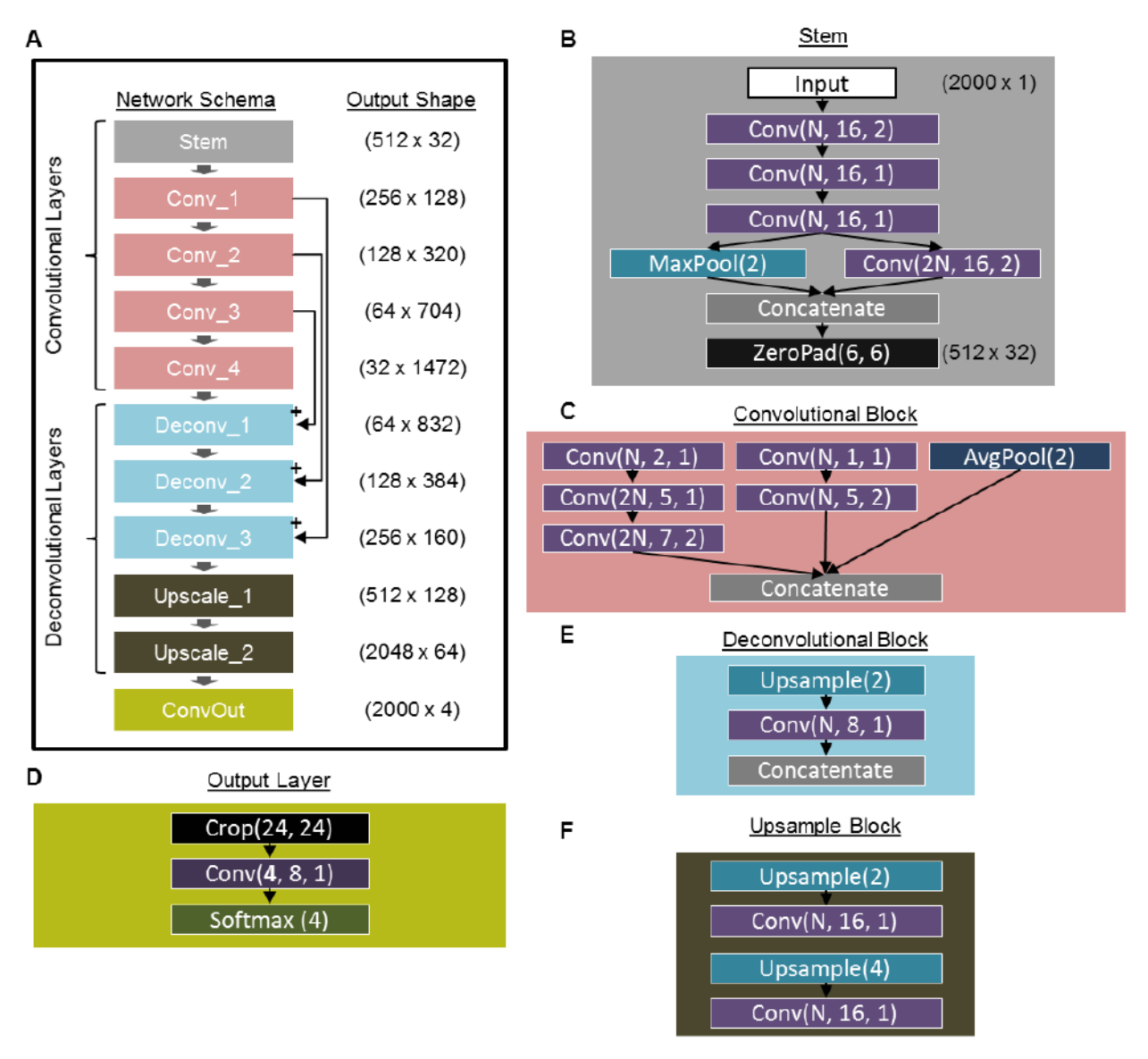


Figure S5. Convolutional neural network architecture. A) High-level network schema of the classification model for 4-class semantic segmentation. B) The first block of the network down samples the signals, and up scales to 512 x 32. This is followed by four C) convolutional blocks, which further down sample the signal. E) Deconvolutional units upscale the signal, followed by F) upsampling blocks, and finally, the D) output layer.

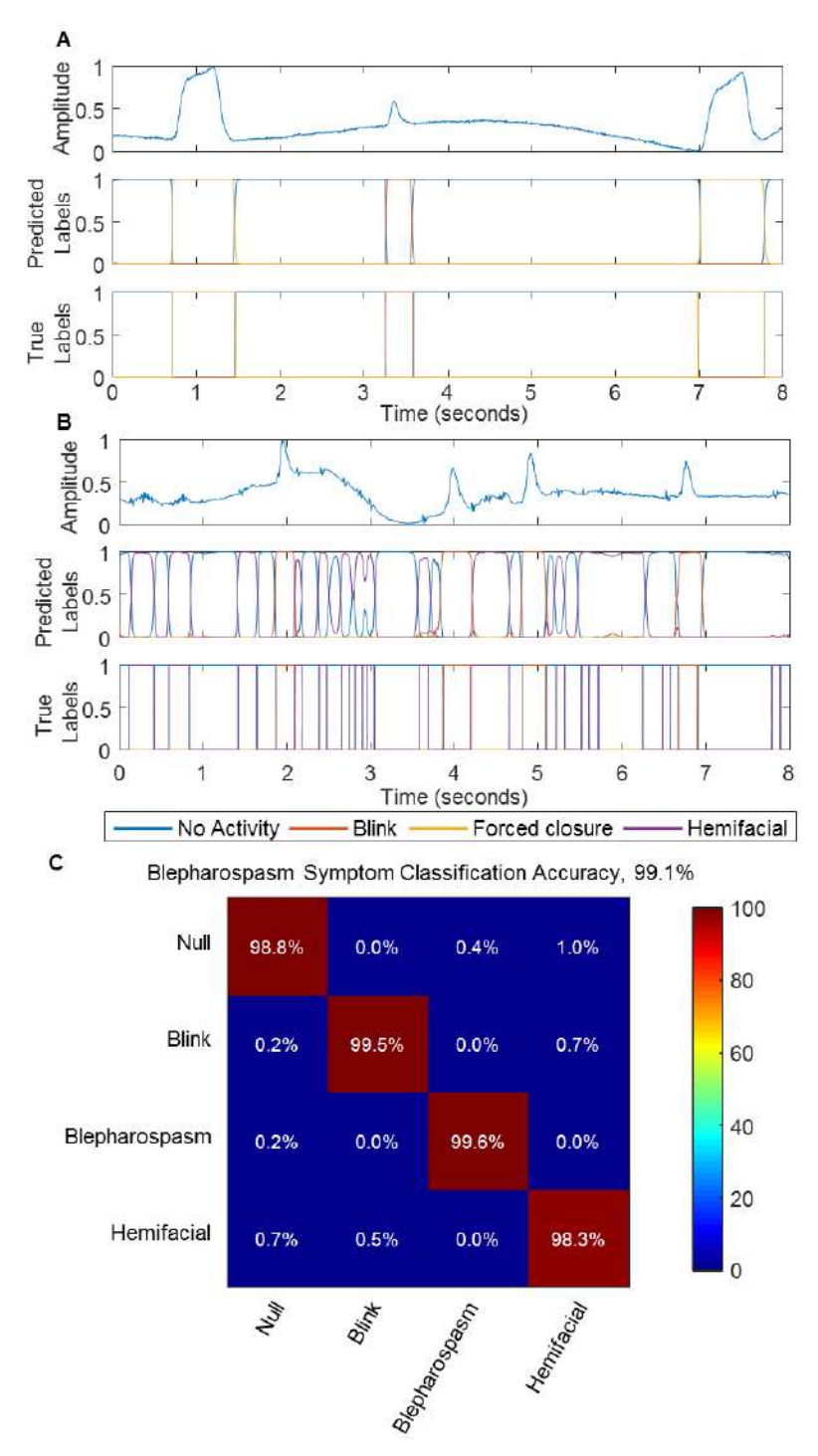


Figure S6. Validation of CNN segmentation. An example in A) shows a successful segmentation of an 8-second window with two forced eye-closures and one blink in a BL patient. B) More complex example showing a patient with pathological blinking, along with subtle hemifacial spasm, which are accurately marked. C) Overall accuracy (99.1%) of the 4-class semantic segmentation scheme.

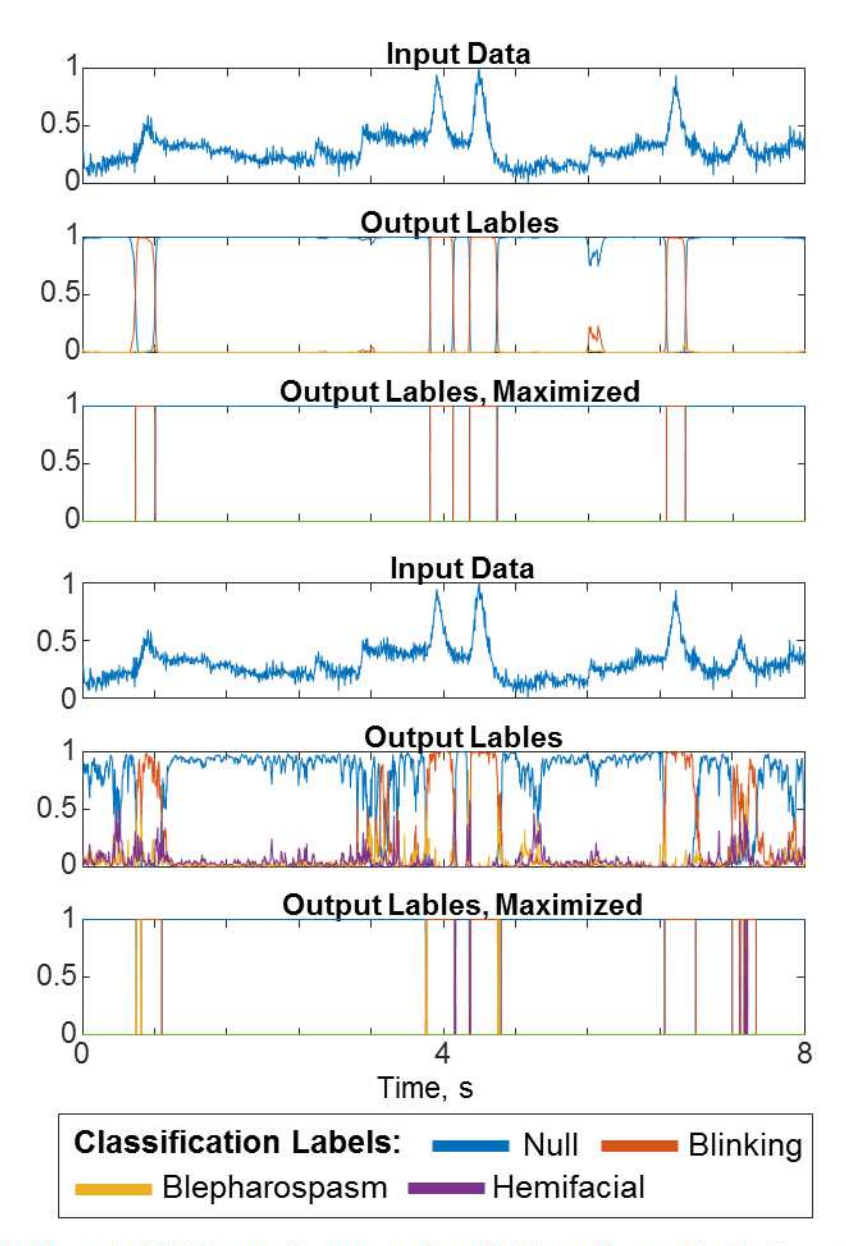


Figure S7. Limitations of CNN Semantic approach and alternative methods. Detection of hemifacial spasms is difficult due to determining the origin of high-frequency muscle activity. In the above sample, there exists a baseline noise, which may be from facial muscles but is not certain. Additionally, these symptoms can overlap with other symptoms (blinks, eye spasms), and the semantic segmentation CNN is not designed to assign multiple labels.

Table S1. List of chip components for a flexible circuit. The table summarizes the component symbol, matching the symbols used in Fig. S1, description, value and part number.

| Component | Description | Value | Part number |
|----------------------------------|--------------------------------------|---------------------|-----------------|
| U1 | 3.3 voltage regulator | N/A | TPS63001 |
| U2 | Analog front-end | N/A | ADS1292 |
| U3 | Bluetooth PSoC | N/A | NRF52832-QFAA-R |
| U4 | Current limit active-low load switch | N/A | TPS22941 |
| L1 | 0402 inductor | 2.2 μΗ | N/A |
| L3 | 0402 inductor | 15 nH | N/A |
| L4 | 0603 inductor | 10 μΗ | N/A |
| L5 | 0402 inductor | 10 nH | N/A |
| L6 | 0402 inductor | 2.7 nH | N/A |
| C1, C10, C14, C15 | 0402 ceramic capacitor | 10 μF | N/A |
| C2 | 0402 ceramic capacitor | 22 μF | N/A |
| C3, C5 | 0402 ceramic capacitor | 4.7 nF | N/A |
| C4 | 0402 ceramic capacitor | 1.0 nF | N/A |
| C6, C7, C12, C22, C26, C33 | 0402 ceramic capacitor | 0.1 μF | N/A |
| C8, C11, C13 | 0402 ceramic capacitor | 1.0 μF | N/A |
| C9 | 0402 tantalum capacitor | 1.0 μF | N/A |
| C21 | 0402 ceramic capacitor | 4.7 μF | N/A |
| C23 | 0603 ceramic capacitor | 10 μF | N/A |
| C24, C25, C28, C29 | 0402 ceramic capacitor | 12 pF | N/A |
| C31 | 0402 capacitor | 0.4 pF | N/A |
| R1, R2, R3, R4 | 0402 resistor | 30 kΩ | N/A |
| R5, R6, R7, R8 | 0402 resistor | $1\mathrm{M}\Omega$ | N/A |
| A1 | 2.45 GHz RF chip antenna | N/A | 2450AT18A100 |
| F1 | 2.45 GHz low pass filter | N/A | 2450FM07A0029 |
| X1 | 32 MHz crystal | N/A | ECS-320-8-37CKM |
| X2 | 32.768 kHz crystal | N/A | ECS327-9-12-TR |
| J1 | Ground connection | N/A | N/A |
| J2 | Battery positive connector | N/A | N/A |
| Ј3 | ADC bias connector | N/A | N/A |
| J4 | ADC channel 1 positive input | N/A | N/A |
| J5 | ADC channel 1 negative input | N/A | N/A |
| J6 | Microcontroller I/O pin | N/A | N/A |
| J7 | Microcontroller CLK pin | N/A | N/A |

 ${\bf Table~S2.~Quantitative~assessment~of~BL~electrophysiological~data~recorded~with~SKINTRONICS.}$

| Subject ID# | Avg. Blink Length (s) | Avg. Eye Spasm Length (s) | Avg. Facial Spasm Length (s) | Blinks/min | Eye Spasms/min | Facial Spasms/min |
|----------------|--------------------------|------------------------------|---------------------------------|------------|-------------------|----------------------|
| S1 | 0.32 ± 0.01 | 0.74±0.07 | 0 | 21.25 | 6.47 | 0 |
| S2 | 0.37±0.01 | 0.54±0.09 | 0 | 29.64 | 2.39 | 0 |
| S3 | 0.44 ± 0.01 | 0.18±0.10 | 0 | 59.23 | 1.85 | 0 |
| S4 | 0.59±0.03 | 0.64±0.34 | 0 | 31.97 | 3.09 | 0 |
| S5 | 0.36 ± 0.02 | 0.46±0.10 | 0 | 44.5 | 4 | 0 |
| S6 | 0.36±0.03 | 0.29±0.10 | 0 | 31.36 | 6.72 | 0 |
| S 7 | 0.31±0.01 | 0.40±0.11 | 0 | 71.57 | 1.08 | 0 |
| S8 | 0.31±0.01 | 0.31±0.02 | 0 | 30.03 | 1.88 | 0 |
| S 9 | 0.31±0.01 | 0.96±0.32 | 0.16±0.02 | 37.5 | 2.25 | 28.5 |
| S10 | 0.46 ± 0.05 | 0.57±0.08 | 0 | 33.68 | 36.81 | 0 |
| S11 | 0.36 ± 0.01 | 0.32±0.05 | 0 | 65.3 | 15.76 | 0 |
| S12 | 0.46±0.02 | 0.56±0.21 | 0 | 34.99 | 3.24 | 0 |
| S13 | 0.43±0.01 | 0.26±0.24 | 0 | 23.71 | 0.95 | 0 |

References

